Ocean Systems Engineering, *Vol. 14, No. 2 (2024) 101-114*
https://doi.org/10.12989/ose.2024.14.2.101

Deep neural network based seafloor sediment mapping using bathymetric features of MBES multifrequency

Khomsin*[1], Mukhtasor[1], Suntoyo[1] and Danar Guruh Pratomo[2]

[1]*Department of Ocean Engineering, ITS Surabaya, Indonesia*
[2]*Department of Geomatics Engineering, ITS Surabaya, Indonesia*

(Received October 20, 2023, Revised December 12, 2023, Accepted December 15, 2023)

Abstract. Seafloor sediment mapping is an essential research topic in shallow coastal waters, especially in port development, benthic habitat mapping, and underwater communications. The seafloor sediments can be interpreted by collecting sediment samples directly in the field using a grab sampler or corer. Another method is optical, especially using underwater cameras and videos. Both methods each have weaknesses in terms of area coverage (mechanic) and accurate positioning (optic). The latest technology used to overcome it is the acoustic method (echosounder) with Global Navigation Satellite System (GNSS) Real Time Kinematic (RTK) positioning. Therefore, in this study will propose the classification of seafloor sediments in coastal waters using acoustic method that is Multibeam Echosounder (MBES) multi-frequency with five frequency (200 kHz, 250 kHz, 300 kHz, 350 kHz, and 400 kHz). In this study, the deep neural network (DNN) used the bathymetric multi frequency, bathymetric difference inters frequencies, and bathymetric features from 5 (five) frequencies as input layer and 4 (four) sediment types in 74 (seventy-four) sample sediment as output layer to make a seafloor sediment map. Results of sediment mapping using the DNN method show an overall accuracy of 71.6% (significant) and a kappa coefficient of 0.59 (moderate). The distribution of seafloor sediment in the study area is mainly silt (41.6%), followed by clayey sand (36.6%), sandy silt (14.2%), and silty sand (7.5%).

Keywords: bathymetric difference; clayey sand; kappa coefficient; overall accuracy; sandy silt; silt; silty sand

1. Introduction

Coastal areas (coastlines, beaches and coastal environments) have been known to attract people for thousands of years and continue to do so today. Many human activities are concentrated in this coastal area, as evidenced by the many large cities with dense populations growing there. Coastal activities require nautical charts to support economic and environmental activities on the coast. Nautical charts are essential in providing data and marine information and describing the seabed and coastline (NOAA 1997).

Nautical charts contain graphical information about the sea and coastal areas, including sea depths, seabed sediments, natural, and artificial shores, navigational hazards, natural aids to navigation, and artificial tides, currents, and man-made structures (IHO 2005). In addition, equally important information that must be included in a nautical chart is the characteristics of seafloor

*Corresponding author, Ph.D., E-mail: khomsin@geodesy.its.ac.id

http://www.techno-press.org/?journal=ose&subpage=7 ISSN: 2093-6702 (Print), 2093-677X (Online)

sediments (Garlan *et al*. 2018). Characteristics of seafloor sediments are an essential research topic in shallow coastal waters, such as hydrology, marine and coastal spatial planning, marine engineering (dredging, underwater, cable and road laying pipes), harbor development, benthic habitat mapping, and underwater communications (Penros *et al*. 2005). The interpretation, classification, and distribution of seafloor sediments can be accomplished by collecting sediment samples directly in the field using a grab or corer. However, of course, this requires much effort in terms of time and cost, which results in low resolution. Another method is optical, especially using underwater cameras and videos (Fonseca and Calder 2005). However, this method needs to be improved due to the difficulty of underwater positioning and the high turbidity of groundwater, leading to clearer image and video results. Additionally, it is difficult to identify different sedimentary boundaries due to sampling over considerable periods. Therefore, more than these methods are needed to meet the needs of modern marine research and development (Zheng *et al*. 2013). Therefore, more than these two methods are needed to map seafloor sediments over large areas and on large scales.

The weakness of the above method lies in the use of underwater acoustic technologies such as single beam echosounder (SBES), side-scanning sonar (SSS), and multibeam echo sounder (MBES). At first, this acoustic technology was only used for bathymetric mapping of the seafloor (SBES and MBES) and seafloor imaging (SSS). The development of acoustic technology for measuring water depth began with SBES and MBES. Over the past two decades, multibeam echosounders have significantly increased the efficiency, accuracy, and spatial resolution of coastal and ocean mapping (Hell 2011). MBES is also a commonly used acoustic tool for observing and mapping the water column and seafloor (Lamarche and Lurton, 2018, Khomsin *et al*. 2021).

MBES data commonly used for sediment classification are monospectral and multispectral backscatter data (Brown *et al*. 2017, Feldens *et al*. 2018, Gaida *et al*. 2018, Brown *et al*. 2019). Multifrequency MBES is an instrument that can be used to carry out surveys based on ping-to-ping, which means emitting acoustic wave signals alternately from one frequency to another. According to Gaida *et al*. (2018) tested this method using multifrequency MBES backscatter (MBES R2Sonic 2026) to better distinguish the acoustic response of seafloor sediments compared to using single-frequency data. Typically, researchers only use backscatter data (Pratomo *et al*. 2018, Ji *et al*. 2020, Zhang *et al*. 2022, Nitriansyah and Cahyono 2022), which combines bathymetry and backscatter data reverse (Zakariya *et al*. 2018, Janowski *et al*. 2018, Xu *et al*. 2021, Wan *et al*. 2022) to determine sediment classification. Some researchers still only use MBES bathymetric data to classify seafloor sediments. This study will propose the classification of seafloor sediments in coastal waters using bathymetric and bathymetric derivatives MBES multifrequency using deep neural networks. There is expected to be a positive correlation between bathymetric and bathymetric derivative and seafloor sediment types.

2. Materials and methods

Multifrequency MBES survey was carried out in the coastal shallow water at PT. Gresik Jasa Tama (PT. GJT) port (Fig. 1), located in Gresik Regency, East Java Province, Indonesia, on Wednesday, 4 January 2023. The survey area is about 41 ha and is a port for loading and unloading wooden ships. The depth in the survey area is from -2.5 m to -25.5 m LWS.

This study acquired seabed backscatter using an R2Sonic 2020 MBES, with the sonar head deployed through a moon pool in the side-mounted survey vessel. Survey dilaksanakan dengan

Fig. 1 Research Survey Location at PT. Gresik Jasa Tama, Gresik Regency, East Java, Indonesia

Table 1 Characteristic of R2Sonic 2020 MBES used during acquisitions (R2Sonic 2020)

Frequency	200 – 450 kHz; 700 kHz optional
Number of soundings	Up to 1024 soundings per ping
Beam width (Ω_{tx} and Ω_{rx})	1° x 1° at 700 kHz (optional); 1.8° x 1.8° at 450 kHz; 4° x 4° at 200 kHz
Selectable Swath sector	10° to 130° User selectable in real-time
Nominal pulse Length τ_n	15 µs – 1 ms
Pulse type	Shape CW
Sounding Pattern	Equiangular Equidistant single / double / quad modes Ultra High Density (UHD

menggunakan mbes multifrekuensi dengan basis ping by ping. At the time of the survey, the MBES system collected data alternately with frequencies of 200, 250, 300, 350, and 400 kHz with equiangular mode. The system settings are all accessible to the user or predefined in automatic acquisition modes such as transmit power, gain, and pulse length.

Table 1 shows the technical characteristics of the R2Sonic 2020 MBES and some parameters used during the acquisition. This system uses differential GNSS for horizontal positioning and heading and an Inertial Motion Unit (IMU) sensor to measure the vessel's attitude (pitch, roll, and yaw). In addition, it is also equipped with tidal observations during the survey to correct chart datum and sound velocity profiler (SVP) measurements at the beginning, middle, and end of the survey to obtain a correction for the speed of sound waves underwater.

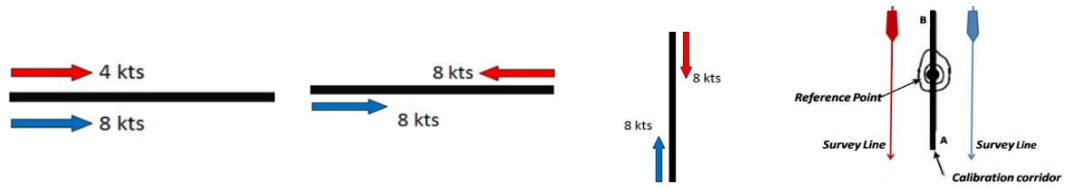

(a) (b) (c) (d)

Fig. 2 Setup for patch test survey (a) latency, (b) pitch, (c), roll (d) yaw (Hoy and Kissinger 2010)

This research method generally consists of collecting, processing, and analyzing. The first step is setting all survey equipment in the data collection. The next step is to measure the patch test (Fig. 2) to calibrate the transducer's alignment to the ship's attitude (pitch, roll, yaw, and latency). The patch test data is first processed to get the latency, pitch, roll, and yaw correction angles. Latency is calibrating time first to eliminate a source of error while conducting the other tests. Run one line twice, in the same direction, at two different speeds (Fig. 2(a)). Pitch can use the same coincident lines as the time delay. It must include a 10-20o slope with a flat surface on each side (Fig. 2(b)). The roll must be conducted on a flat bottom to show the same offset in the port and starboard outer beams (Fig. 2(c)). The object of yaw should be centered between the two lines and half the distance of each line (Fig. 2(d)). SVP data is used for sound velocity correction underwater, and tidal data is used to correct datum reference. Patch test, SVP, and tidal data were entered into each survey data line to get the data corrected.

The next step is splitting the data into five files containing one frequency and data editing to eliminate existing noise. Finally, multifeature multispectral backscatter is input and sediment sample type as output to the deep neural network to classify seabed sediments. The DNN in this study used a multi-layer perceptron (MLP) with five hidden layers, each consisting of 45 neurons and one output layer containing four neurons, each representing the seabed classes. The activation function was set to the rectified linear unit (ReLU) for hidden layers due to its simplicity, speed, and ability to prevent gradient vanishing problems (Agarap 2019). As for the output layer, the softmax function was used as the activation function. The function is selected since it constrains the sum values of all neurons in the output layer to be equal to 1, ensuring the probability at each neuron lies in the range of 0 to 1. In optimization, the Adam optimizer, which applies an adaptive learning rate and moment, was used (Kingma and Ba 2015), and the loss function was set to categorical cross-entropy. Hence, to prevent the overfitting problem, a dropout strategy and L1+L2 regularization were employed. In addition, the maximum number of epochs was 100. However, the epochs which stored the highest accuracy were extracted using a model check-point technique and further used for seabed classification.

Furthermore, based on previous experiments, models that use datasets to train 70% of the population and test 30% of the population can achieve the best accuracy. In this study, the hyperparameter tuning, including the activation function, loss function, optimizer, and regularization, was set based on the theoretical approach. Detailed information on hyperparameter tuning is described in chapter 3.

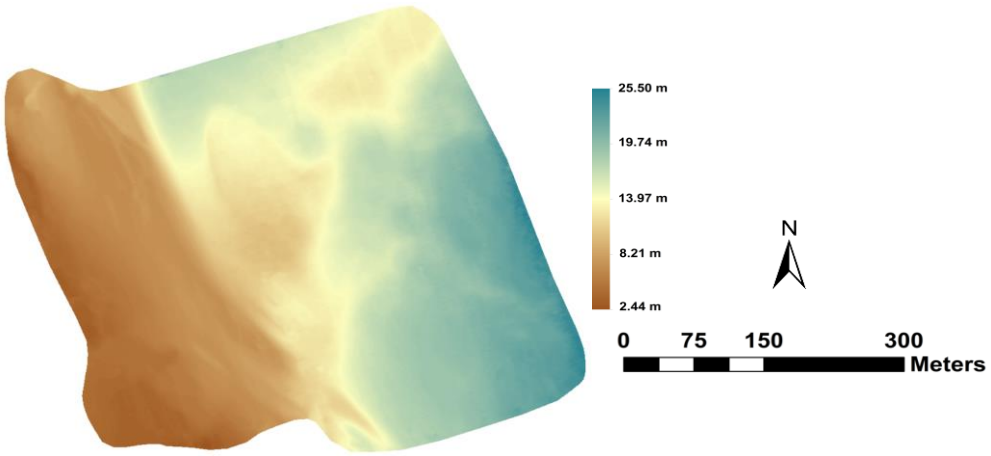

Fig. 3 Digital Bathymetric Model in Area Survey for 200 kHz

Table 2 Patch Test Mounting Results

Calibration Type	Area Used	Result
Time	No area	0 s
Pitch	177.59 m^2	-0.95^0
Roll	31.32 m^2	0.63^0
Heading	10.85 m^2	-0.45^0

3. Result and discussion

3.1 Patch test

Sensors' misalignment or mistiming relative to one another can create dynamic residuals and a static bias (e.g., roll bias). The patch test aims to align the transducer with the existing reference system on the ship, namely by calculating the rotation angle concerning the y-axis (roll), the x-axis (pitch), and the z-axis (yaw), and latency. Most installations will incorporate GNSS time synchronization, and no latency is expected in the GNSS position. Roll measurement is carried out on one survey line, measured back and forth twice and at the same survey speed. An error in the roll will result in an error in sounding depths. Pitch measurement is the same as roll, measured back and forth and at the same speed but seabed slope. The effect of pitch error increases significantly with depth in the along-track position. The yaw test uses two parallel lines with the ship in the same direction on the line. Yaw error will happen in-depth position error, which increases far from the nadir. Table 2 shows the patch test results where the pitch is -0.95^0, the roll is 0.63^0, and the heading is -0.45^0. The patch test values (pitch, roll, and heading) and latency should be entered into the appropriate areas in the data collection.

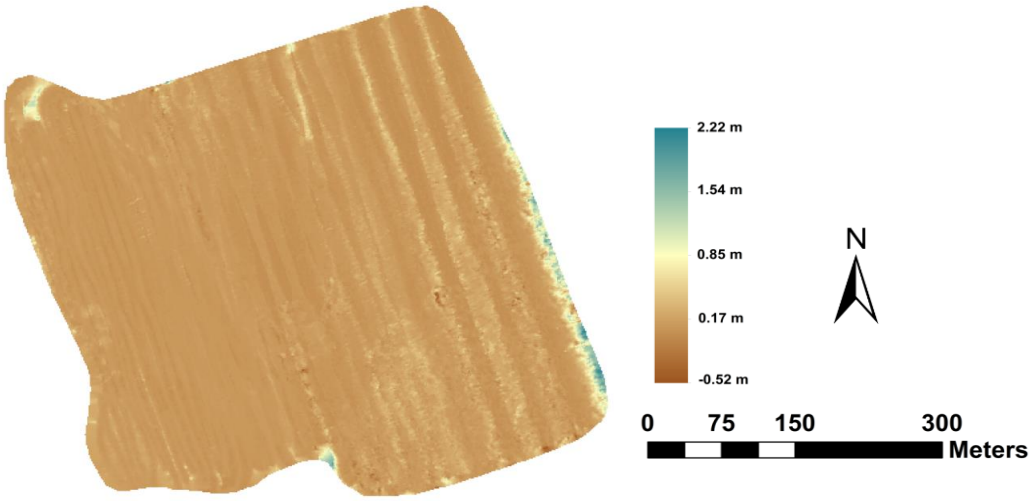

Fig. 4 Difference bathymetric inter frequencies between 200 kHz and 400 kHz

3.2 Digital bathymetric model

The survey results using R2Sonic 2020 multifrequency MBES with frequencies of 200 kHz, 250 kHz, 300 kHz, 350 kHz and 400 kHz after correction with patch test data (latency, pitch, roll and yaw), sound wave correction (SVP), tidal correction (against datum reference) and noise will produce bathymetric data for each frequency. One of the digital bathymetric data is shown in Fig. 3.

Fig. 3 shows the depth in the survey area (GJT port) is from 2.44 m LWS to 25.5 m LWS. The area on the beach (around the port pool) is the area in the west has a depth of 2.44 m LWS to 8.21 m LWS; the area on the west, which is the western shipping channel area of Surabaya, shows a depth of more than 13.97 m LWS to 25.5 m. Meanwhile, the middle area, the channel to the port pool, has a depth of 8.2 1 m LWS to 13.97 m. This shows that the GJT port area can still accommodate ships with a draft of 2.5 m at the time of the most receding conditions. With a tide interval of 2.5 meters, ships with a draft of 5 m can enter at the highest tide.

3.3 Difference bathymetric inter frequency

Each bathimetric data of each frequency (200 kHz, 250 kHz, 300 kHz, 350 kHz, and 400 kHz) is subtracted with each other. Fig. 4 shows the difference in bathimetry between frequency depths of 200 kHz and 400 kHz. In general, a frequency of 200 kHz has a deeper depth than the depth of 400 kHz frequency.

Generally, in the area survey, the difference between 200 kHz depth and 400 kHz depth ranges from 0 m to 0.85 m (light brown to yellow). However, there are some areas (very small) where the depth difference between 200 kHz and 400 kHz is negative (dark brown). In addition, there are some locations where the depth difference is more than 0.5 m (yellow to blue). Depth differences that are negative and more than 50 cm can be due to noise by interpolation.

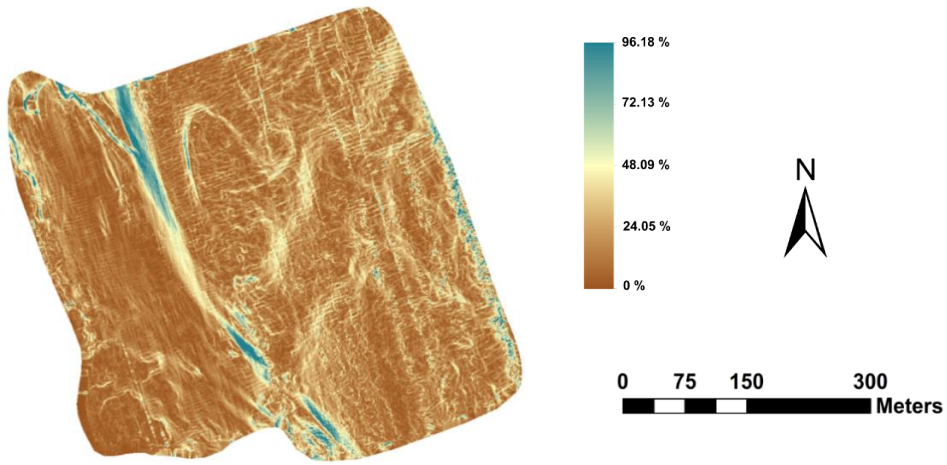

Fig. 5 Slope the area survey with 200 kHz

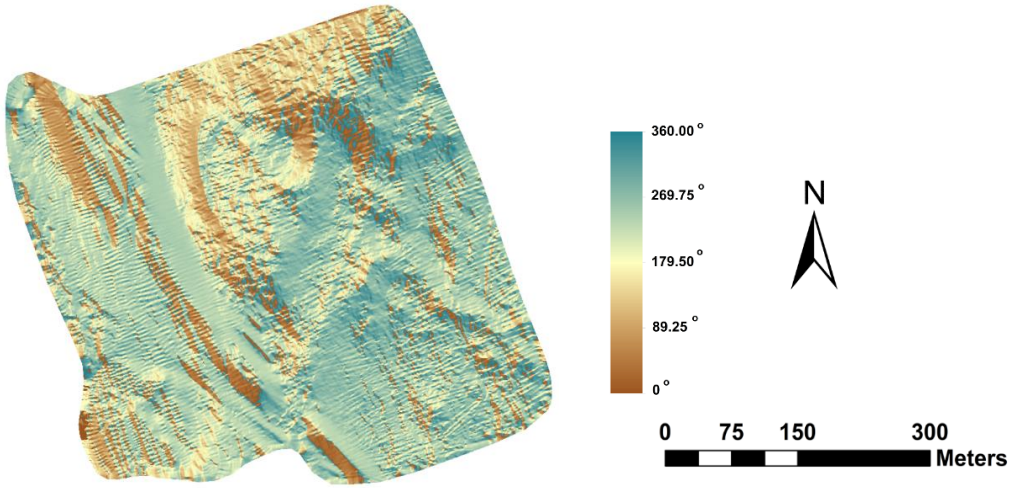

Fig. 6 Aspect of bathymetric feature with frequency 300 kHz

3.4 Bathymetric feature

3.4.1 Slope

The slope is the change in elevation from one point to another expressed by a gradient (m). The unit of slope can be both degrees and even percent. According to Van Zuidam (1983), slopes are classified as flat (0% - 8%), gentle slope (2% - 7%), sloping (7% - 15%), moderately steep (15% - 30%), steep (30% - 70%), very steep (70% - 140%) and extremely steep (> 140%). Fig. 5 shows the slope in the survey area which is dominated by less than 15% (flat – gentle slope with brown), 15% – 70% (moderately steep – steep with light brown – yellow – light green), and over 70% (very steep with green). The very steep area is a hard sediment (gravel or rock), so this area is not easy to slide.

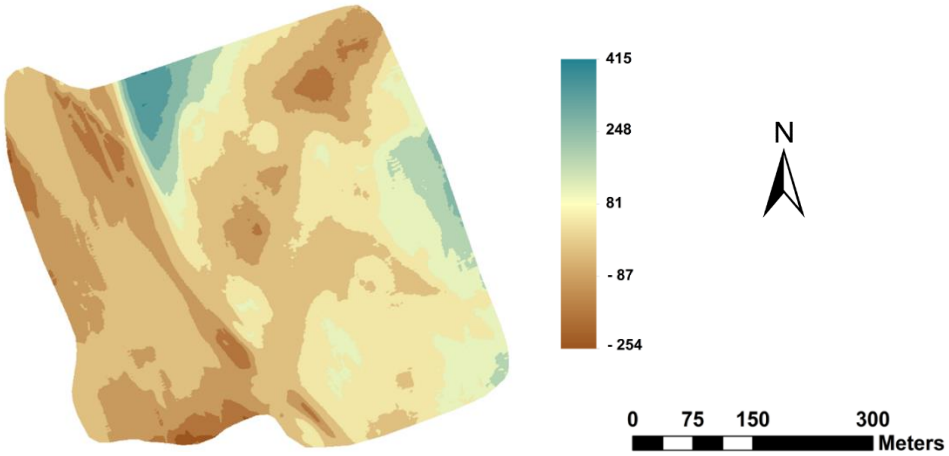

Fig. 7 Bathymetric Position Index (BPI) feature with frequency 400 kHz

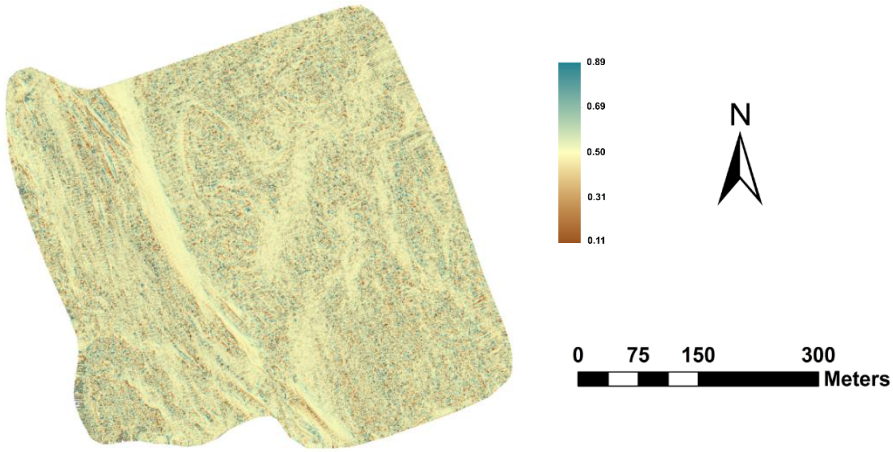

Fig. 8 Roughness of bathymteric feature with frequency 250 kHz

3.4.2 Aspect

Aspect is a bathimetric feature that shows the direction of inclination expressed by degrees. According to Kobryn (2022) grouped aspects into classes: east (45 – 135), south (135 – 225), west (225 – 315) and north (315 – 360 and 0 – 45). The aspect of bathymetric features in the survey area is dominated by north (green / 315 - 360) and brown (0 - 45), west 9 light green) and south (yellow). From this aspect, it is indicated that sedimentary movement is dominated towards the north.

3.4.3 Bathymetric position index

Bathymetric Position Index (BPI) is a bathimetric feature that shows the referenced position relative to the surrounding location. BPI will show negative values (valley), flat (zero or close to 0) and ridge (ridge). Fig. 7 shows the BPI in the survey area which has -254 to 415. Light brown color

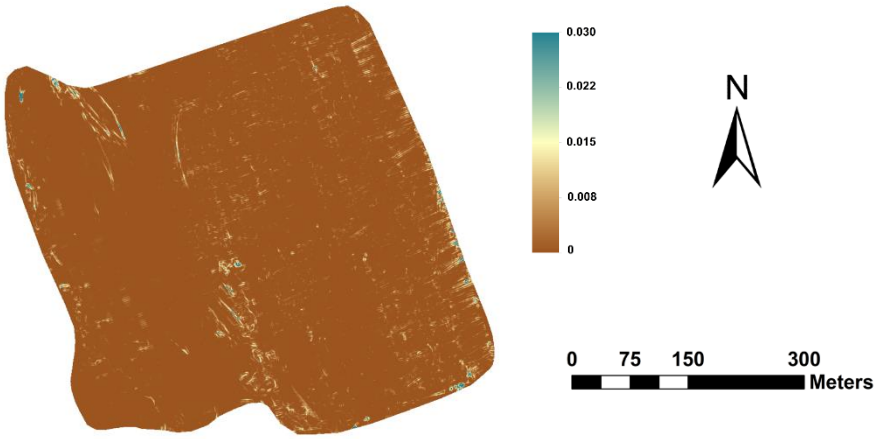

Fig. 9 Ruggedness of bathymteric feature with frequency 400 kHz

with a value of about zero indicates that the area is flat, areas with brown color indicate valley areas and yellow to green colors indicate areas with ridge terrain.

3.4.4 Roughness

The roughness of the seafloor surface is the deviation of the depth value from the average depth around it. The roughness value in the survey area showed a value of 0.11 m – 0.89 m. In general, the roughness value in the survey area dominated by ranges from 0.40 m – 0.60 m.

3.4.5 Ruggedness

Ruggedness is a measure of the variation in local location on the seafloor about the central pixel. The ruggedness value is calculated by comparing a central pixel to its neighbors, taking the absolute value of the difference value, and averaging the results. Fig. 9 shows ruggedness in the survey area with values from 0 – 0.030. The survey area is dominated by brown which has a value of about 0.

3.4.6 Curvature

Curvature is a derivative of bathymetric data that aims to see the seabed basin in an upward or downward direction. Describes the steepest curve of either plan or profile convexity through a defined cell neighbourhood. The survey area is dominated by curvature with a value of -9.18 m-1 (Fig. 10).

3.5 Seafloor sediment predicted map

The technique used to predict the distribution map of bottom sediments in the waters of Gresik Jasa Tama Port is a deep neural network. Deep neural networks are machine learning using artificial neural network systems. A deep neural network (DNN) is a feedforward with data flowing from the input layer to the outer layer without feedback. At first, DNNs assigned random numerical values, or commonly referred to as "weights", to connections between artificial neurons. Then the weight and input data are multiplied and produce an output between 0 and 1 according to the activation

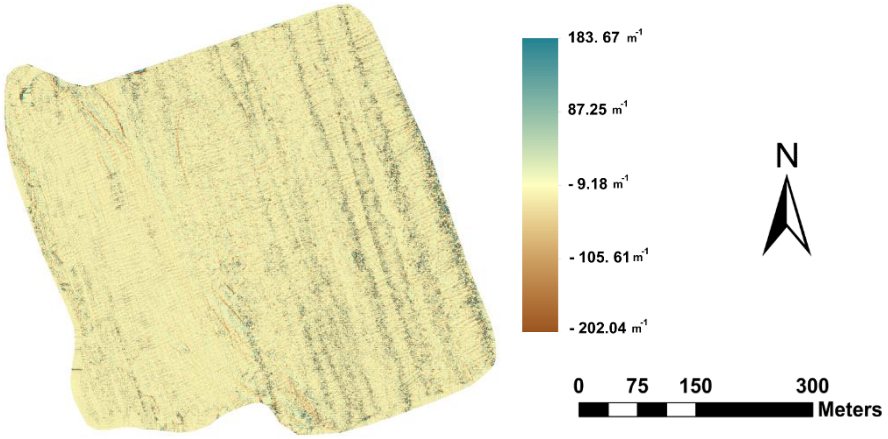

Fig. 10 Curvature of bathymteric feature with frequency 200 kHz

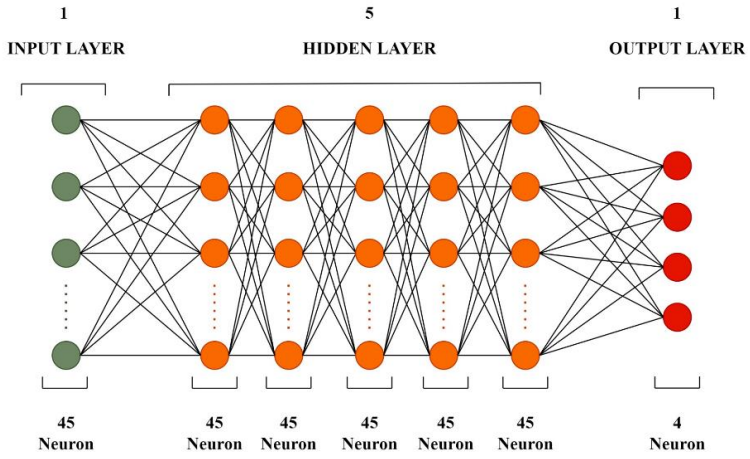

Fig. 11 Deep Neural Network Model Classifer with 45 neurons

function used. If the network has not been able to accurately recognize certain patterns used for the learning process, the algorithm will recalculate and adjust the weight value. DNN has several things that need to be set to be able to carry out pre-planned functions and can provide optimal performance (Arif, 2020). In this case, there are as many as 45 data that are used as input layers, namely 5 frequency bathimetric data (5 layers), bathimetric differences between frequencies (10 layers), and 6 bathimetric features for each frequency (5 x 6 = 30 layers).

Fig. 11 shows the diagram of a multi-layer perceptron (MLP) with five hidden layers, which is used in this paper. Each hidden layer consists of forty-five neurons. The activation functions used are reLU for the hidden layers and softmax for the output layer. The algorithm of the value of DNN properties, such as weights and learning rate, estimates the adaptive moment estimation. Some experiments and models use datasets to train 70% of the population and test 30% to achieve

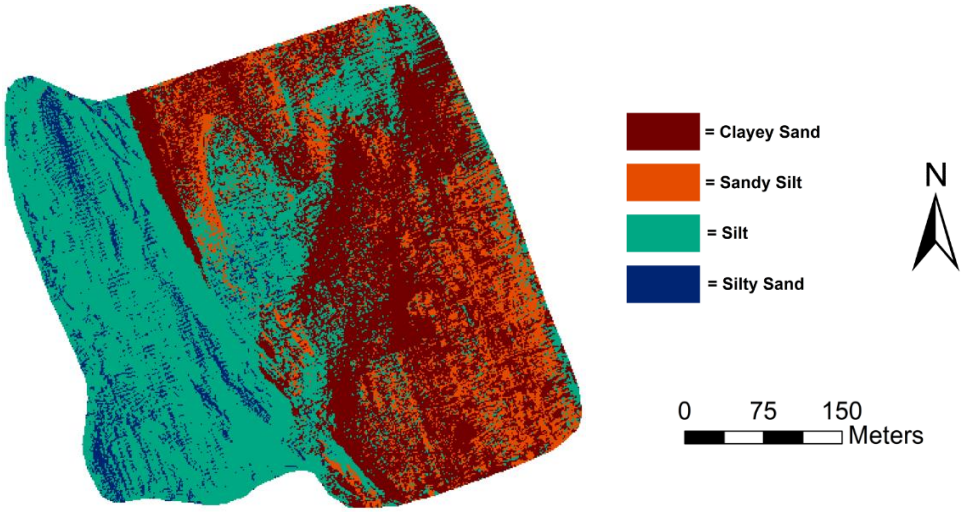

Fig. 12 Predicted Seabed Sediment with DNN in the survey area

maximum accuracy. Generally, the model with reLU activation function (hidden layer) and softmax activation function (output layer) achieve 98.39% training accuracy and 75% testing accuracy. It is generated using a batch size setting of 1, a learning rate setting of 0.0001, and an epoch parameter of 74.

The results of the seabed sediment prediction maps in the survey area using DNN can be seen in Fig. 12. Seabed sediments in GJT port are dominated by silt (41.6%), which spreads around the port pool (western area), and clayey sand (36.6%) in the size of the eastern part (western shipping channel of Surabaya). A small portion of the site around the harbor with silty sand (7.5%) and sandy silt (14.2%) sediments spread over the outer east side of the survey area.

A confusion matrix can assess the results accuracy of seabed sediment prediction for accuracy. The confusion matrix (Table 3) is a matrix that contains a cross table between in situ (as a reference) and prediction data (Foody 2002). There are four parameters used to evaluate prediction results, namely producer accuracy (PA), user accuracy (UA), overall accuracy (OA), and Kappa coefficient (Cohen 1960). User accuracy (UA) is the relationship between the prediction class and all in situ data, and conversely, the relationship between the correct prediction value and all pixel classes is called producer accuracy (PA) (Story and Congalton 1986, Congalton 1991).

The overall accuracy equals the sum of all correctly classified instances over all instances in the confusion matrix. Overall accuracy tells us which proportions were mapped correctly out of all the reference locations. Overall accuracy, with an accuracy of 100, is a perfect classification level where all reference locations have been correctly classified. The Kappa coefficient considers the possibility of agreement occurring by chance (Cohen 1960). The Kappa coefficient evaluates how well the classification performed compared to randomly assigning values ranging from -1 to 1.

In this study, the high PA value was silt class (92.6%) with 25 types of Silt in reference (in situ) matching 27 samples, while UA was Sandy Silt (100%), with only five prediction class points matching the in-situ sample class. The user and producer accuracy for any given class is typically different. In this case, the producer's accuracy for the Silt class was 92.6%, while the user's accuracy was 64.1%. It means that even though 92.6% of the reference silt areas have been correctly identified

Table 3 Confusion Matrix of Classification Seabed Sediment with DNN

		Reference (In Situ)					
		Clayey Sand	Sandy Silt	Silt	Silty Sand	Total	UA
Predicted	Clayey Sand	17	3	1	1	22	77.3
	Sandy Silt	0	5	0	0	5	100
	Silt	5	2	25	7	39	64.1
	Silty Sand	0	1	1	6	8	75
	Total	22	11	27	14	74	
	PA	77.3	45.4	92.6	42.9		
	OA	71.6%					
	Kappa	0.59					

as Silt, only 64.1% percent of the areas identified as Silt in the classification were Silt. The overall accuracy value in this case is 71.6%, where are 53 samples suitable for all classes with details of clayey sand 17, sandy silt 5, silt 25, and silty sand 6, with a total sample of 74. At the same time, the value of the Kappa coefficient is 0.59. The Kappa value of 0.59, according to Landis and Koch (1977) included in the strength of agreement 'moderate,' and the overall accuracy value of 71.6% falls into the substantial category.

While increasing the volume of data typically enhances model reliability, previous studies have primarily relied on extensive datasets obtained through established techniques such as angular range analysis (ARA), Bayesian methods, and other classification approaches for seabed characterization (Mertikas and Karantzalos 2020, Ntouskos *et al*. 2023). Although utilizing simulated data may mitigate data scarcity issues, achieving convergence to the global minimum of the loss function presents a formidable challenge, potentially compromising model accuracy. Hence, we advocate for utilizing ground-truth data to ensure precision and reliability in our analysis.

4. Conclusions

The results of bathymetric surveys with multifrequency R2Sonic MBES with frequencies of 200 kHz, 250 kHz, 300 kHz, 350 kHz, and 400 kHz showed that the depth in GJT waters ranged from 2.4 m LWS to 25.5 m LWS. The depth difference between frequencies is dominated by depth difference values ranging from 0 – 50 cm. The bathymetric features of each frequency in the form of the slope, aspect, BPI, roughness, ruggedness, and curvature show the same appearance and relative values between frequencies. The classification of in situ sediment samples as 74 sample points shows the classes of clayey sand, silt, silty sand, and sandy silt. The results of sediment mapping using the DNN method with 45-layer inputs (bathymetry (5), bathymetric differences (10), and bathymetric features of each frequency (30)) and layer outputs in the form of clayey sand, silt, silty sand, and sandy silt showed that the overall accuracy was 71.6% (substantial) and kappa coefficient 0.59 (moderate). The distribution of bottom sediment in the survey area was dominated by silt (41.6%) and followed by clayey sand (36.6%), sandy silt (14.2%) and silty sand (7.5%).

Acknowledgements

We thank our colleagues from PT. APBS provided insight and expertise that greatly assisted the research related to the R2Sonic2020 multi-frequency MBES survey and Eiva Corporation, which has licensed the Navi Edit JobPlanner and Navi Model Producer software to the geomatics engineering department. Not to forget, we also thank PT. GJT has allowed GJT waters as a survey area.

References

Agarap, A.F.M. (2019), "Deep Learning using Rectified Linear Units (ReLU)", arXiv:1803.08375v2. [cs.NE]

Arif, T.M. (2020), Introduction to Deep Learning for Engineers: Using Python and Google Cloud Platform. (Synthesis Lectures on Mechanical Engineering). Morgan & Claypool, Vol. 5.

Brown, C.J., Beaudoin, J., Brissette, M. and Gazzola, V. (2017), "Setting the Stage for Multispectral Acoustic Backscatter Research" *WHITE PAPER*. R2Sonic.

Brown, C.J., Beaudoin, J., Brissette, M. and Gazzola, V. (2019), "Multispectral multibeam echo sounder backscatter as a tool for improved seafloor characterization", *Geosciences*, **9***(*3), 126 MDPI. https://doi.org/10.3390/geosciences9030126.

Cohen, J. (1960), "A coefficient of agreement for nominal scales", *Educational and Physicological Measurement*, **20**(1). 37-46. https://doi.org/10.1177/001316446002000104.

Congalton, R.G. (1991), "A review of assessing the accuracy of classifications of remotely sensed data", *Remote Sens. Environ*., **37**, 35-46. https://doi.org/10.1016/0034-4257(91)90048-B.

Feldens, P., Schulze, I., Papenmeier, S., Schönke, M. and Schneider von Deimling, J. (2018), "Improved interpretation of marine sedimentary environments using multi-frequency multibeam backscatter data", *Geosciences*, **8**(6), 214. https://doi.org/10.3390/geosciences8060214.

Fonseca, L. and Calder, B. (2005), "Geocoder: an efficient backscatter map constructor", *Proceedings of the U.S. Hydrographic Conference*, San Diego.

Foody, M.G. (2002), "Status of land classification accuracy", *Remote Sens. Environ.*, **80**(1). 185-201. https://doi.org/10.1016/S0034-4257(01)00295-4.

Gaida, T.C., Ali, T.A.T., Snellen, M., Simkooei, A.A., van Dijk, T.A.G.P. and Simons, D.G. (2018), "A multispectral bayesian classification method for increased acoustic discrimination of seabed sediments using multi-frequency multibeam backscatter data", *Geosciences*, **8**, 455. MDPI. https://doi.org/10.3390/geosciences8120455.

Hell, B. (2011), "Mapping bathymetry: From measurement to applications", Doctoral thesis in Marine Geoscience. Department of Geological Sciences Stockholm University, Stockholm Sweden.

Hoy, S. and Kissinger, K. (2010), "Multibeam calibration: Conducting a patch test NOAA ship Okeanos explorer", OER Interns

IHO (2005), *Manual on Hydrography Publication M-13 1st Ed.*, Monaco: International Hydrographic Bureau

Janowski, L., Tęgowski, J. and Nowak, J. (2018), "Seafloor mapping based on multibeam echosounder bathymetry and backscatter data using Object-Based Image Analysis: A case study from the Rewal site, the Southern Baltic", *Int. J. Oceanography Hydrobiol*., **47**(3). https://doi.org/10.1515/ohs-2018-0024.

Ji, X., Yang, B. and Tang, Q. (2020), "Seabed sediment classification using multibeam backscatter data based on the selecting optimal random forest model", *Appl. Acoust.*, **167**, 107387. https://doi.org/10.1016/j.apacoust.2020.107387.

Kingma, D.P. and Ba, J.L. (2015), Adam: A Method for Stochastic Optimization. ICLR. arXiv:1412.6980v9 [cs.LG].

Kobryn, H.T., Beckley, L.E. and Wouters, K. (2022), "Bathymetry derivatives and habitat data from hyperspectral imagery establish a high-resolution baseline for managing the Ningaloo Reef, Western Australia", *Remote Sens*., **14**, 1827. https://doi.org/10.3390/rs14081827.

Landis, R.J. and Koch, G.G. (1977), "The measurement of observer agreement for categorial data", *Biometrics*, **33**(1), 159- 174. https://doi.org/10.2307/2529310.

Lamarche, G. and Lurton, X. (2018), "Recommendations for improved and coherent acquisition and processing of backscatter data from seafloor-mapping sonars", *Mar. Geophys. Res*., **39**, 5-22. https://doi.org/10.1007/s11001-017-9315-6.

Mertikas, P. and Karantzalos, K. (2020), "Seafloor mapping from multispectral multibeam acoustic data at the European open science cloud", *Int. Archiv. Photogramm. Remote Sens. Spatial Inform. Sci*., 2020, XXIV ISPRS Congress (2020 edition). https://doi.org/10.5194/isprs-archives-XLIII-B2-2020-985-2020.

Nitriansyah, R. and Cahyono, B.K. (2022), "Seabed classification using multibeam echosounder measurement data", *IOP Conf. Ser.: Earth Environ. Sci.*, 1039 012045. https://doi.org/10.1088/1755-1315/1039/1/012045.

NOAA (1997), *Nautical Chart User's Manual. U.S. Department of Commerce National Oceanic and Atmospheric Administration (NOAA)* National Ocean Service. United State of America.

Ntouskos, V., Mertikas, P., Mallios, A. and Karantzalos, K. (2023), "Seabed classification from multispectral multibeam data", *IEEE J. Oceanic Eng*., **48**(3), https://doi.org/10.1109/JOE.2023.3267795.

Penrose, J.D., Siwabessy, P.J.W., Gavrilov, A., Parnum, I., Hamilton, L.J., Bickers, A., Brooke, B., Ryan, D.A., and Kennedy, P. (2005), *Acoustic Techniques for Seabed Classification*, Cooperative Research Centre for Coastal Zone Estuary and Waterway Management. Technical Report 32.

Pratomo, D.G. (2021), "The development of seafloor sediment mapping methods: The opportunity application in the coastal waters", *IOP Conf. Ser.: Earth Environ. Sci*., **731**, 012039. https://doi.org/10.1088/1755-1315/731/1/012039.

Pratomo, D.G., Khomsin, Cahyadi, M.N., Akbar, K. and Aprilia, E. (2018), "Analysis of seafloor sediment Distribution using Multibeam Backscatter Data", *MATEC Web of Conferences*, **177**, 01026. https://doi.org/10.1051/matecconf/201817701026.

R2Sonic (2020), *Multibeam Echosounder Specifications*. 5307 Industrial Oaks Blvd. Suite 120. Austin, Texas 78735, USA.

Story, M. and Congalton, R.G. (1986), "Accuracy assessment: A user's perspective", *Photogramm. Eng. Remote Sens.*, **52**, 397-399.

Van Zuidam, R.A. (1973), *Guide to Geomorphologic-Aerial Photographic Interpretation and Mapping*, International Institute for Geo-Information Science and Earth Observation, ITC. Enschede, Netherland.

Wan, J., Qin, Z., Cui, X., Yang, F., Yasir, M., Ma, B. and Liu, X. (2022), "MBES seabed sediment classification based on a decision fusion method using deep learning model", *Remote Sens.*, **14**, 3708. https://doi.org/10.3390/rs14153708.

Xu, W., Cheng, H., Zheng, S. and Hu, H. (2021), "Predicted mapping of seabed sediments based on MBES backscatter and bathymetric data: A case study in Joseph Bonaparte Gulf, Australia, using random forest decision tree", *J. Mar. Sci. Eng.*, **9**, 947. https://doi.org/10.3390/jmse9090947.

Zakariya, R., Abdullah, M.A., Hasan, R.C. and Khalil, I. (2018), "The use of backscatter classification and bathymetry derivatives from multibeam data for seabed sediment characterization", (Ed., Öchsner, A.), *Eng. Appl. New Mater. Tech*., **85**. https://doi.org/10.1007/978-3-319-72697-7_47

Zhang, Q., Zhao, J., Li, S. and Zhang, H. (2022), "Seabed sediment classification using spatial statistical characteristics", *J. Mar. Sci. Eng*., **10**, 691. https://doi.org/10.3390/jmse10050691.

Zheng, H.B., Yan, P., Chen, J. and Wang, Y.L. (2013), "Seabed sediment classification in the northern South China sea using inversion method", *Appl. Ocean Res*., **39**, 131-136. https://doi.org/10.1016/j.apor.2012.11.002.